AIP | Physics of Plasmas

Verification of gyrokinetic particle simulation of current-driven instability in fusion plasmas. I. Internal kink mode

J. McClenaghan, Z. Lin, I. Holod, W. Deng, and Z. Wang

Citation: Physics of Plasmas (1994-present) **21**, 122519 (2014); doi: 10.1063/1.4905073
View online: http://dx.doi.org/10.1063/1.4905073
View Table of Contents: http://scitation.aip.org/content/aip/journal/pop/21/12?ver=pdfcov
Published by the AIP Publishing

Verification of gyrokinetic particle simulation of current-driven instability in fusion plasmas. I. Internal kink mode

J. McClenaghan, Z. Lin,[a] I. Holod, W. Deng,[b] and Z. Wang[c]
University of California, Irvine, California 92697, USA

(Received 26 September 2014; accepted 17 November 2014; published online 30 December 2014)

The gyrokinetic toroidal code (GTC) capability has been extended for simulating internal kink instability with kinetic effects in toroidal geometry. The global simulation domain covers the magnetic axis, which is necessary for simulating current-driven instabilities. GTC simulation in the fluid limit of the kink modes in cylindrical geometry is verified by benchmarking with a magneto-hydrodynamic eigenvalue code. Gyrokinetic simulations of the kink modes in the toroidal geometry find that ion kinetic effects significantly reduce the growth rate even when the banana orbit width is much smaller than the radial width of the perturbed current layer at the mode rational surface. © *2014 AIP Publishing LLC*. [http://dx.doi.org/10.1063/1.4905073]

I. INTRODUCTION

Large currents are needed to form nested magnetic surfaces for confining high temperature plasmas in axisymmetric fusion devices. These equilibrium currents often excite magnetohydrodynamic (MHD) instabilities including ideal kink modes[1] and resistive tearing modes.[2] The basic physics mechanisms of these current-driven instabilities manifest themselves in tokamak plasmas as various macroscopic MHD modes, such as fishbones,[3] sawteeth,[4] neoclassical tearing modes,[5] and resistive wall modes,[6] which can limit burning plasma performance and threaten fusion device integrity.[7] The studies of the MHD modes typically rely on MHD simulations[8–10] or reduced models.[11] However, the excitation and evolution of macroscopic MHD modes often depend on kinetic effects at microscopic scales and on the nonlinear coupling of multiple physical processes, e.g., microturbulence, neoclassical transport, and energetic particle effects. Therefore, fully self-consistent simulations require a kinetic approach to incorporate microscopic kinetic effects in these current-driven MHD modes. In this work, we extend gyrokinetic particle simulation[12] capability to the internal kink instability with kinetic effects in toroidal geometry.

The ideal MHD internal kink mode is an $m = n = 1$ perturbation driven unstable by gradients of the equilibrium currents in magnetized plasmas. Here, m and n are the poloidal and toroidal, respectively, mode number. The mode structure peaks at the rational surface with the safety factor $q = 1$ in a tokamak. While internal kink modes are observed to be relatively benign in tokamaks,[1] they can trigger fishbone modes and sawtooth oscillations, both are a potential threat to the α-particle confinement in the International Thermonuclear Experimental Reactor (ITER). The excitation of fishbone-like modes[13,14] by fast ions is routinely observed in current tokamak experiments. Recently, experiments manipulate the current profile to destabilize the sawtooth oscillations to avoid the more dangerous neoclassical tearing modes.[15] When q is larger than unity but approaches unity, a long-lived kink mode has been observed to degrade the fast ion confinement.[8,16,17]

The ideal MHD theory finds that the internal kink is always unstable in a cylindrical geometry with a $q = 1$ surface.[1] In a toroidal geometry, the internal kink mode can be stabilized by the toroidicity[18] due to the coupling to the $m = 2$ harmonic. However, the toroidicity can be either stabilized or destabilized depending on the plasma beta β (defined as the ratio of kinetic pressure to magnetic pressure).[19] The stabilization of internal kink modes by the toroidicity has been confirmed in some MHD simulations.[20,21] Recently, nonlinear two-fluid simulations with sources and sinks were able to demonstrate the long time dynamics of kink modes exhibiting sustained cycles.[22]

Kinetic effects can play an important role on the stability of the internal kink mode due to the thin layer of perturbed currents near the mode rational surface.[1] The kinetic effects tend to stabilize the internal kink mode[23,24] in general. However, sufficient fast ion pressure gradients can destabilize internal kink modes[25] or even excite fishbone modes.[26] To study the kinetic effects, gyrokinetic particle simulation has been utilized to simulate internal kink modes in the cylindrical geometry.[27,28] The growth rate and mode structure are found[29] to depend strongly on the ratio of ion gyroradius to radial width of the perturbed current layer near the rational surface. In the toroidal geometry, a gyrokinetic eigenvalue analysis[30] shows that trapped ions can significantly affect the internal kink eigenmode structure and growth rate.

Here, we extend the global gyrokinetic toroidal code (GTC)[31,32] capability for simulating internal kink modes, for the first time, with kinetic effects in the toroidal geometry. GTC has been extensively applied to study neoclassical and turbulent transport[33,34] and energetic particles.[35] It has recently been extended to simulate kinetic-MHD processes including various Alfvén eigenmodes.[36,37] The implementation of the

[a]Author to whom correspondence should be addressed. Electronic mail: zhihongl@uci.edu
[b]Present address: Princeton Plasma Physics Laboratory, Princeton University, Princeton, New Jersey 08543, USA.
[c]Present address: Oak Ridge Associated Universities, General Atomics, San Diego, California 92121, USA.

equilibrium current and the verification of its effects on reverse shear Alfvén eigenmode[38] enable GTC simulation of current-driven instabilities, such as kink modes reported in this paper and tearing modes in a follow-up paper.[39] In the present work, we first extend the simulation domain to magnetic axis for global kink simulation. We then verify GTC simulations of internal kink modes in the cylindrical geometry by benchmarking with an MHD eigenvalue code. Finally, GTC gyrokinetic simulations of internal kink modes in the toroidal geometry find that ion kinetic effects significantly reduce the growth rate even when the banana orbit width is much smaller than the radial width of the perturbed current layer.

The structure of the paper is as follows. In Sec. II, the simulation method will be described, including extension of the simulation domain to the magnetic axis. In Sec. III, GTC simulations of the internal kink mode in the cylindrical geometry are verified. Toroidal simulations are presented in Sec. IV. Conclusions and discussions are given in Sec. V.

II. GYROKINETIC SIMULATION MODEL FOR KINETIC MHD

A. Gyrokinetic formulation with equilibrium current

Since the frequency and growth rate of kinetic-MHD modes are much smaller than the ion cyclotron frequency, nonlinear gyrokinetics, which removes unwanted high frequency modes and rigorously retains all linear and nonlinear wave-particle resonances and finite Larmor radius effects, is well suited to study kinetic-MHD modes.

Using δ as a smallness parameter, the gyrokinetic ordering is[40–42]

$$\frac{\omega}{\Omega_i} \sim k_\parallel \rho_i \sim \frac{\delta B}{B_0} \sim k_\perp \rho_i \frac{e\delta\phi}{T} \sim \mathcal{O}(\delta). \tag{1}$$

The variables ω, $k_\parallel$, and $k_\perp$ are wave frequency, parallel wave vector, and perpendicular wave vector of the mode of interest; Ω_i, ρ_i, and B_0 are ion cyclotron frequency, ion Larmor radius, and equilibrium magnetic field; δB, $\delta\phi$, and T are perturbed magnetic field, perturbed electrostatic potential, and plasma temperature.

Since the electron mass is much smaller than the ion mass, the electron dynamics are on a much faster time scale compared to the ion dynamics. Due to the computational time constraints, it is often impractical to calculate the brute force electron dynamics for macroscopic MHD modes. This motivated the fluid-kinetic hybrid electron model in which the electron distribution function is expanded using the smallness parameter of the ratio of wave frequency to electron transit frequency.[43] In the zeroth order, the electrons are adiabatic and can be described by the continuity equation (i.e., massless electron model). Nonadiabatic responses are treated kinetically in the higher order. However, in this paper only massless electrons will be considered since the important kinetic effects (finite orbit width, wave-particle resonances, and polarization drift) on the kink instability are mostly contributed by ions. The fluid-kinetic hybrid electron model removes collisionless tearing mode physics from the simulation, and avoids well known numerical difficulties associated with tearing mode physics.[44] In extension to this model, GTC simulations of resistive tearing modes using the fluid electron model with a resistivity term have recently been verified.[39] The collisionless tearing mode using a finite-mass electron model has also been verified.[45]

Starting with the electron fluid and field equations for the fluid-kinetic hybrid model, the nonlinear continuity equation derived from the drift kinetic equation is[38]

$$\begin{aligned}
&\frac{\partial n_e}{\partial t} + \mathbf{B}_0 \cdot \nabla\left(\frac{n_{0e}\delta u_{\parallel e}}{B_0}\right) + B_0 \mathbf{v}_\mathbf{E} \cdot \nabla\left(\frac{n_{0e}}{B_0}\right) \\
&-n_{0e}(\delta \mathbf{v}_{*\mathbf{e}} + \mathbf{v}_\mathbf{E}) \cdot \frac{\nabla B_0}{B_0} + \delta\mathbf{B} \cdot \nabla\left(\frac{n_{0e}u_{\parallel 0e}}{B_0}\right) \\
&+\frac{c\nabla \times \mathbf{B}_0}{B_0^2} \cdot \left[-\nabla \delta P_{\parallel e} + n_{0e}\nabla\delta\phi\right] \\
&+\delta\mathbf{B} \cdot \nabla\left(\frac{n_{0e}\delta u_{\parallel e}}{B_0}\right) + B_0 \mathbf{v}_\mathbf{E} \cdot \nabla\left(\frac{\delta n_e}{B_0}\right) \\
&+\frac{c\delta n_e}{B_0^2}\mathbf{b}_0 \times \nabla B_0 \cdot \nabla\delta\phi + \frac{c\delta n_e}{B_0^2}\nabla \times \mathbf{B}_0 \cdot \nabla\delta\phi = 0,
\end{aligned} \tag{2}$$

where the electron density n_e and the electron parallel flow $u_{||e}$ are split into the equilibrium and perturbed quantities: $n_e = n_{0e} + \delta n_e$ and $u_{||e} = u_{||0e} + \delta u_{||e}$. The drift velocities are defined as $\mathbf{v}_\mathbf{E} = \frac{c\mathbf{b}_0 \times \nabla\delta\phi}{B_0}$ and $\mathbf{v}_{*\mathbf{e}} = \frac{\mathbf{b}_0 \times \nabla\left(\delta P_{\parallel e} + \delta P_{\perp e}\right)}{n_{0e}B_0}$, where $\mathbf{b}_0$ is the unit vector along the direction of the equilibrium magnetic field, $\delta P_{||e}$ and $\delta P_{\perp e}$ are the parallel and perpendicular perturbed electron pressure, and c is the speed of light.

Using the Padé approximation, the gyrokinetic Poisson equation is[40]

$$\frac{c^2}{4\pi v_A^2}\nabla_\perp^2 \delta\phi = -\left(1 - \rho_i^2\nabla_\perp^2\right)\left(Z_i\overline{\delta n}_i - \delta n_e\right), \tag{3}$$

where $\overline{\delta n}_i$ is the perturbed gyro-averaged ion density, v_A is the Alfvén velocity, and Z_i is the ion charge. Gyrokinetic Ampere's law is used to calculate the electron perturbed current

$$n_{0e}e\delta u_{\parallel e} = \frac{c}{4\pi}\nabla_\perp^2 A_\parallel + Z_i n_{0i}\overline{\delta u}_{\parallel i}. \tag{4}$$

The variable $\overline{\delta u}_{||i}$ is the perturbed parallel ion flow. The perturbed magnetic potential $\delta A_{||}$, defined as $\delta\mathbf{B} = \nabla \times \delta A_\parallel \mathbf{b}_0$, is calculated from

$$\frac{\partial \delta A_{||}}{\partial t} = -\mathbf{b}_0 \cdot \left(\delta\phi - \delta\phi_{eff}\right), \tag{5}$$

where the effective scalar potential, which describes the parallel electric field ($\delta E_{||} = \mathbf{b}_0 \cdot \nabla\phi_{eff}$), in the lowest order is

$$\delta\phi_{eff} = eT_e\frac{\delta n_e}{n_{0e}} - \frac{\delta\psi}{n_{0e}}\frac{\partial n_{0e}}{\partial\psi_0}. \tag{6}$$

This effective potential comes from the non-ideal ion kinetic effects (e.g., ion polarization drift and wave-particle interactions). The parallel and perpendicular perturbed electron pressures in the lowest order are

$$\delta P_{||e} = \delta P_{\perp e} = n_{0e} e \delta \phi_{eff} + \frac{\partial (n_{0e} T_e)}{\partial \psi_0} \delta \psi, \tag{7}$$

where ψ_0 and $\delta\psi$ are the equilibrium and perturbed poloidal flux, respectively.

When ion kinetic effects are suppressed and parallel electric field is set to zero, Eqs. (2)–(7) form a closed system, which will be referred to as GTC fluid simulation from now on. Also, for the fluid limit linear simulations the $\mathbf{v}_E$ terms in the electron continuity equation are removed because they cancel out with the ions. This set of equations has been shown to recover reduced MHD.[38]

To incorporate the kinetic effects from the ions, the ion flow $\overline{\delta u_i}$ and the ion density $\overline{\delta n_i}$ are calculated using the gyrokinetic equation

$$\frac{d}{dt} f_i(\mathbf{X}, \mu, v_{\|}, t) \equiv \left[\frac{\partial}{\partial t} + \nabla \cdot \dot{X} + \dot{v}_{\|} \frac{\partial}{\partial v_{\|}} \right] f_i = 0. \tag{8}$$

The term f_i is the ion gyrocenter distribution function, $\dot{\mathbf{X}}$ is the position of the gyrocenter, $v_{||}$ is the velocity parallel to the magnetic field, and μ is the magnetic moment.

The ion gyrocenter motion is governed by

$$\dot{\mathbf{X}} = v_{\|} \mathbf{b} + \mathbf{v}_E + \mathbf{v}_d, \tag{9}$$

$$\dot{v}_{\|} = -\frac{1}{m_i} \frac{\mathbf{B}^*}{B_0} \cdot (\mu \nabla B_0 + Z_i \nabla \delta \phi) - \frac{Z_i}{m_i} \frac{\partial \delta A_{\|}}{\partial t}, \tag{10}$$

where m_i is the ion mass. The magnetic field is

$$\mathbf{B}^* = \mathbf{B}_0^* + \delta \boldsymbol{B} = \mathbf{B}_0 + \frac{B_0 v_{\|}}{\Omega_i} \nabla \times \mathbf{b}_0 + \delta \boldsymbol{B}, \tag{11}$$

where magnetic drift velocity $\mathbf{v}_d$ is the sum of the curvature drift $\mathbf{v}_c$ and grad-B drift $\mathbf{v}_g$

$$\mathbf{v}_d = \mathbf{v}_c + \mathbf{v}_g = \frac{v_{\|}^2}{\Omega_i} \nabla \times \mathbf{b}_0 + \frac{\mu}{m_i \Omega_i} \mathbf{b}_0 \times \nabla B_0. \tag{12}$$

B. Equilibrium model

In this subsection, a brief description of the equilibrium model is given. GTC uses a magnetic flux coordinate system (ψ, θ, ζ), where ψ is the poloidal magnetic flux, θ is the poloidal angle, and ζ is the toroidal angle. The covariant and contravariant representations of the magnetic field and the Jacobian $\mathcal{J}$ are shown below[46]

$$\mathbf{B}_0 = g(\psi) \nabla \zeta + I(\psi) \nabla \theta = q \nabla \psi \times \nabla \theta - \nabla \psi \times \nabla \zeta, \tag{13}$$

$$\mathcal{J}^{-1} = \nabla \psi \cdot (\nabla \theta \times \nabla \zeta) = \frac{B_0^2}{gq + I}. \tag{14}$$

The parameters q, $2\pi g$, and $2\pi I$ are the safety factory, poloidal current, and toroidal current, respectively. Using the covariant representation of the magnetic field, the equilibrium current density can be written as

$$\nabla \times \mathbf{B}_0 = g' \nabla \psi \times \nabla \zeta + I' \nabla \psi \times \nabla \theta. \tag{15}$$

While GTC has the capability to simulate realistic tokamak equilibria,[37,47] this paper will focus on using analytical equilibria to simulate kink modes for both cylindrical geometry and toroidal geometry. In cylindrical geometry, the toroidal angle is defined as $\zeta = 2\pi z/L$, where z is the axial position and L is the length of the cylinder. The effective major radius in cylindrical geometry is $R_0 = L/2\pi$, and a periodic boundary condition is used for the toroidal angle. The cylindrical geometry equilibrium is

$$\begin{aligned} B_0 &= B_a, \\ I &= B_a r^2/q, \\ g &= B_a R_0^2, \\ \theta &= \theta_0, \\ \zeta &= \zeta_0, \end{aligned} \tag{16}$$

where B_a is the on axis magnetic field strength. The variables θ_0 and ζ_0 represent the geometric poloidal and toroidal angles and ϵ is the local inverse aspect ratio $\epsilon = r/R_0$.

For toroidal simulations, a tokamak with concentric flux-surfaces will be used at two levels of approximation.[48] At the lowest order in the expansion of the toroidal geometry, using the inverse aspect ratio as a smallness parameter, we approximate the magnetic flux θ-coordinate as the geometric angle θ_0

$$\begin{aligned} B_0 &= B_a - B_a \epsilon \cos\theta_0 + \mathcal{O}(\epsilon^2), \\ I &= B_a r^2/q + \mathcal{O}(\epsilon^4), \\ g &= B_a R_0^2 + \mathcal{O}(\epsilon^2), \\ \theta &= \theta_0, \\ \zeta &= \zeta_0. \end{aligned} \tag{17}$$

The next order is a realistic toroidal geometry equilibrium,[38] which uses a more realistic magnetic flux θ-coordinate

$$\begin{aligned} B_0 &= B_a - B_a \epsilon \cos\theta_0 + \mathcal{O}(\epsilon^2), \\ I &= B_a r^2/q + \mathcal{O}(\epsilon^4), \\ g &= B_a R_0^2 + \mathcal{O}(\epsilon^2), \\ \theta &= \theta_0 - \epsilon \sin\theta_0, \\ \zeta &= \zeta_0. \end{aligned} \tag{18}$$

Note that a poloidal current term g of order ϵ^2 was ignored, while the toroidal current term I of same order is kept. This is because toroidal current term is an order of ϵ smaller than the poloidal current in the equilibrium current density $\nabla \times \mathbf{B}_0$ because $|\nabla\zeta/\nabla\theta| \sim \epsilon$.

For implementation of the realistic toroidal geometry equilibrium, the Cartesian coordinates $X(\psi, \theta)$ and $Z(\psi, \theta)$ are approximated for construction of a 2D spline. This is done so that each term in the X and Z are separable into a function of ψ and θ, and the 2D splines can be constructed from a 1D spline in ψ and a 1D spline in θ

$$\begin{aligned} X &= 1-\epsilon\cos\theta_0 \approx 1-\epsilon\cos(\theta+\epsilon\sin\theta) \\ &\approx 1-\epsilon\cos\theta+\epsilon^2\sin^2\theta-1/2\epsilon^3\sin^2\theta\cos\theta, \\ Z &= \epsilon\sin\theta_0 \approx \epsilon\sin(\theta-\epsilon\sin\theta) \\ &\approx \epsilon\cos\theta+\epsilon^2\sin\theta\cos\theta-1/2\epsilon^3\sin^2\theta. \end{aligned} \tag{19}$$

C. Extending the simulation region to the magnetic axis

In this subsection, a method to extrapolate solutions to the magnetic axis for the gyrokinetic Poisson equation and Ampere's Law is discussed. The simulation domain must include the magnetic axis, since the $m=n=1$ internal kink mode structures have a finite value near the axis which will be shown in Secs. III and IV. This suggests that the internal kink mode could be unphysically damped by excluding the magnetic axis. GTC uses the finite difference method to calculate the two dimensional perpendicular Laplacian on a poloidal plane away from the magnetic axis. The Laplacian operator in GTC is written in magnetic flux coordinates, as shown below[47]

$$\begin{aligned} \nabla_\perp^2 F = {} & g^{\psi\psi}\frac{\partial^2 F}{\partial\psi^2}+2g^{\psi\theta}\frac{\partial^2 F}{\partial\psi\partial\theta}+\left(g^{\theta\theta}+g^{\zeta\zeta}/q^2\right)\frac{\partial^2 F}{\partial\theta_0^2} \\ & +\frac{1}{\mathcal{J}}\left(\frac{\partial\mathcal{J}g^{\psi\psi}}{\partial\psi}+\frac{\partial\mathcal{J}g^{\psi\theta}}{\partial\theta}\right)\frac{\partial F}{\partial\psi} \\ & +\frac{1}{\mathcal{J}}\left(\frac{\partial\mathcal{J}g^{\psi\theta}}{\partial\psi}+\frac{\partial\mathcal{J}g^{\psi\psi}}{\partial\theta}\right)\frac{\partial F}{\partial\theta}. \end{aligned} \tag{20}$$

In the above equation, the contravariant tensor is defined as $g^{\alpha\beta}\approx\nabla\alpha\cdot\nabla\beta$, where α and β are any combination of the magnetic coordinates ψ, θ, or ζ. The choice of the magnetic flux coordinate system leads to numerical errors when inverting the Laplacian operator near the axis for low-m modes. To understand why the numerical errors arise, consider Laplace's equation in cylindrical coordinates, which has the Bessel functions J_m as a solution. With r being defined as the minor radius, Bessel functions behave as $J_m \propto r^m$ near the axis, and the equilibrium poloidal flux behaves as $\psi \propto r^2$ near the magnetic axis. Since quantities like $\partial r/\partial\psi$ and $\partial^2 r/\partial\psi^2$ are singular near the magnetic axis, the Laplacian of a $m=0$, 1 Bessel function will lead numerical errors in differencing the ψ derivatives.

To avoid numerical errors near the magnetic axis, the Laplacian is solved using finite differences for the majority of the simulation domain, then $\delta\phi$ and $\delta A_{||}$ are extrapolated to the magnetic axis for the first few flux surfaces. The flux surface that separates the finite differences region and the extrapolation region will be referred to as the "FD Boundary" for short. The perpendicular Laplacian of a Bessel function returns the same Bessel function multiplied by a constant with $\nabla_\perp^2 J_m(\eta r)\cos(m\theta) = -\eta^2 J_m(\eta r)\cos(m\theta)$, where η is the numerical constant. This relationship can be used to extrapolate the behavior of $\delta\phi$ and $\delta A_{||}$ near the magnetic axis. The method described here retains only the $m=0$, 1 modes. To extrapolate solutions to the magnetic axis, perturbed quantities such as $\delta\phi$ and $\delta A_{||}$ can be Fourier decomposed at the FD Boundary surface. Since the $m=0$ Bessel function is approximately constant, and the $m=1$ Bessel function is approximately linear in r, the Laplacian of a function near the magnetic axis can be extrapolated with the form of the equation below

$$\nabla_\perp^2 F = a_0 + a_1\frac{r}{r_b}\cos\theta + b_1\frac{r}{r_b}\sin\theta. \tag{21}$$

The quantities a_0, a_1, and b_1, are the poloidal Fourier coefficients of the perturbed quantities at the FD Boundary flux surface. The radial location of the FD Boundary is given by r_b, where the subscript b represents the radial FD boundary grid point. To complete the finite differences Laplacian matrix, a linear boundary condition in r is chosen between the extrapolation region and the finite difference region.

$$F_{b-1} = 2F_b - F_{b+1}. \tag{22}$$

To test this Laplacian operator, with the variable "a" being defined as the minor radius of the wall, the function $F = re^{-50(r/a)^8}$, was chosen because it is linear in r near the magnetic axis. A perpendicular Laplacian is performed analytically on F, and solved for $G = \nabla_\perp^2 F$. The function G is input into GTC, which solves the gyrokinetic Poisson equation for F. The numerical solution to the perpendicular Laplacian and the analytical function F can be seen in Figure 1. For this test case, the first eight radial grid points were chosen to be in the extrapolation region, and the rest in the finite differences region. The GTC solution and the analytic function F agree well in both regions with no significant error near the FD boundary.

To treat the ion dynamics near the magnetic axis, if a particle is located within the flux surface of the first radial grid, the position is updated using Cartesian-like coordinates

$$\begin{aligned} x &= \sqrt{\psi}\cos\theta, \\ z &= \sqrt{\psi}\sin\theta. \end{aligned} \tag{23}$$

The ion position is updated using the following equations:

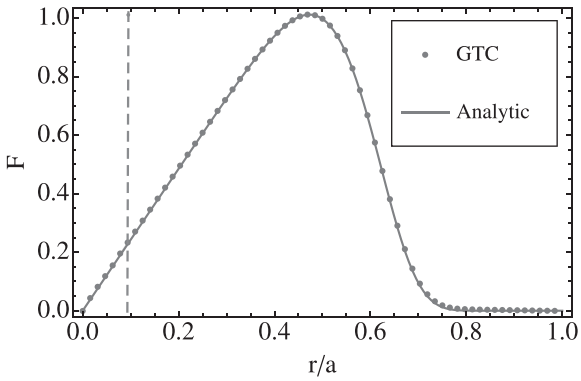

FIG. 1. The GTC laplacian operator solution and the analytic solution for F are plotted against radial coordinate, r/a. The FD boundary flux surface is drawn with a vertical dashed line.

$$x_1 = x_0 + \Delta t\left(\frac{\partial x}{\partial \psi}\dot{\psi} + \frac{\partial x}{\partial \theta}\dot{\theta}\right),$$
$$z_1 = z_0 + \Delta t\left(\frac{\partial z}{\partial \psi}\dot{\psi} + \frac{\partial z}{\partial \theta}\dot{\theta}\right). \quad (24)$$

The subscripts 0 and 1 represent the old and new positions, respectively. The term Δt is the time step size, $\dot{\theta}$ and $\dot{\psi}$ are the time derivatives of the particle position in magnetic coordinates, which are described in detail in Holod *et al.*[32]

III. GTC SIMULATION OF KINK INSTABILITY IN CYLINDRICAL GEOMETRY

The first internal kink mode simulations are in cylindrical geometry in order to verify the gyrokinetic capability of simulating kink modes and to benchmark the GTC results against ideal MHD theory without added complexity of toroidicity. The MHD eigenvalue code used to benchmark the GTC internal kink simulation is based on the 1D solution to the MHD equations in the cylindrical geometry and contains all ideal MHD effects.[49] The GTC fluid limit model contains only the reduced MHD physics making approximations such as $k_{||}/k_{\perp} \ll 1$, and $\delta B_{||} = 0$.

The Alfvén frequency is used to normalize the internal kink growth rate and is defined as $\omega_A = v_A/R_0$. In this simulation, a uniform pressure is used with the ion gyroradius of $\rho_i/R_0 \approx 0.001$ and an electron beta of $\beta_e = 8\pi n_{0e} T_e/B^2 = 0.4\%$. In the MHD eigenvalue code, the finite beta effect that comes from compressibility is found to be negligible. The safety factor is

$$q(r) = \frac{4}{5}\left(1 + \frac{r^2}{a^2}\right), \quad (25)$$

where a is the minor radius of the device.

A. GTC simulations in fluid limit

For the GTC fluid simulations, the linearized equations (2)–(7) are used with ion kinetic effects suppressed and with the parallel electric field set to zero (i.e., $\delta\phi_{eff} = 0$). Since the effective scalar potential is set to zero and there is no equilibrium pressure gradient, β_e does not enter into the system of fluid equations.

Applying an initial perturbation to $\delta A_{||}$, the simulation is ran long enough to observe exponential growth and converged mode structures. Figure 2 shows the growth rate of the internal kink mode for three different inverse aspect ratios. As the inverse aspect ratio increases, the growth rate of the internal kink mode increases for both GTC and MHD eigenvalue codes. For all three aspect ratios, the GTC growth rate agrees with the MHD growth rate to within 15%. This increase in growth rate for larger inverse aspect ratio can be seen in Rosenbluth *et al.*,[1] where it was shown that the internal kink growth rate is of the order $\gamma \sim r^2/R_0^2\,\omega_A$. The frequency from the GTC simulation is zero, which is consistent with the ideal MHD theory.

With radial location of the $q = 1$ mode rational surface defined as r_s, the $r_s/R_0 = 0.25$ case will be examined more closely, since it has the largest growth rate and a broad mode

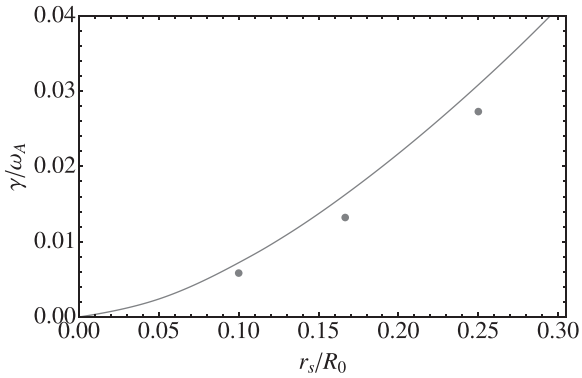

FIG. 2. The internal kink mode growth rate is plotted vs. the inverse aspect ratio r_s/R_0 of the $q = 1$ surface for cylindrical geometry.

width at the mode rational surface. While all m-modes are kept, the $m = 1$ mode is the dominant mode in these simulations. The GTC $m = 1$ mode structures of $\delta A_{||}$, $\delta u_{e||}$, and $\delta\phi$, along with their ideal MHD counterparts are shown in Figures 3 and 4. Overall, the agreement between GTC and ideal MHD mode structures is good, however, the GTC mode structures are slightly sharper at the $q = 1$ surface than the MHD mode structures. In Figure 3, the perturbed current $\delta J_{||}$ has a thin layer that is peaked at the $q = 1$ surface. Defining Δr_{kink} as the half width of this current layer, the current layer width is $\Delta r_{kink}/a \approx 0.061$. It is the size of this current layer that the ion gyroradius and other relevant scale lengths will be compared to in Secs. III B, III C, and IV B.

The small differences in growth rates and mode structure between GTC and MHD eigenvalue codes can likely be attributed to the difference between the two models such as the assumption of $k_{||}/k_{\perp} \ll 1$, and $\delta B_{||} = 0$ in GTC.

B. GTC gyrokinetic simulations

For studying kinetic effects on the internal kink mode for the $r_s/R_0 = 0.25$ case, the same parameters as the fluid simulation are used, where $\beta_e = \beta_i = 0.4\%$. For the gyrokinetic simulations, the linearized equations (2)–(12) are used. In this simulation, the ion Larmor radius is much smaller than the minor radius and the perturbed current layer with $\rho_i/a \approx 0.002$ and $\rho_i/\Delta r_{kink} \approx 0.033$. Since the ion gyroradius scale length is much smaller than relevant mode scale lengths, kinetic effects

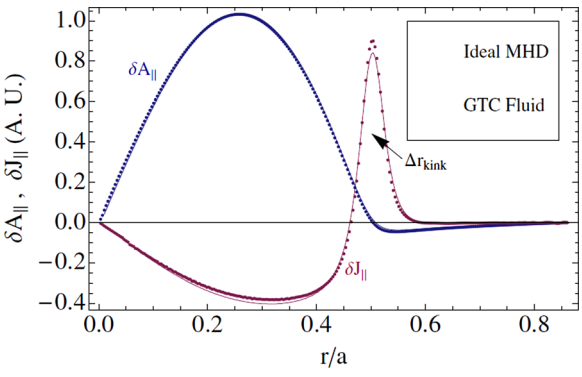

FIG. 3. The mode structure of the $\delta A_{||}$ and $\delta J_{||}$ are plotted against the radial coordinate r/a, for the $r_s/R_0 = 0.25$ case in cylindrical geometry.

should play only a small role and the result should be similar to the fluid simulation.

The internal kink mode growth rate from the kinetic simulation is $\gamma = 0.026\ \omega_A$, about 10% smaller than the fluid simulation. Figure 4 shows the internal kink mode electrostatic potential from GTC gyrokinetic, GTC fluid and MHD simulations. The electrostatic potential in the gyrokinetic simulation is almost identical to the GTC fluid simulation. In the regime where the Larmor radius is much less than the perturbed current layer, the kinetic effects are not significant as expected. This result agrees with Mishchenko and Zocco,[29] which showed that the ion kinetic effects are not important when the ratio of the ion gyroradius to the MHD current layer $\rho_i/\Delta r_{kink}$ is approximately twice the value used in our simulation.

C. Convergence tests

In this subsection, two convergence tests that were performed for GTC fluid simulation of the $r_s/R_0 = 0.25$ case are shown in Figure 5. The first convergence test is to ensure that the FD boundary does not cause any numerical problems. Figure 5(a) shows the internal kink mode growth rate for different values of radial FD boundary point. The growth rate remains almost constant for different r_b, suggesting that the FD radial boundary location has little effect on the growth rate as long as the boundary is far away from the mode $q = 1$ surface. For the rest of the simulations in this paper, a FD boundary point of $r_b = 0.04a$ is chosen where the $q = 1$ surface is at $r = 0.5a$.

The other convergence test is a radial grid point convergence shown in Figure 5(b). Since internal kink modes can have a thin current layer at the $q = 1$ surface, it is important to make sure that the thin layer is adequately resolved. The growth rate is approximately converged when there are 128 radial grid points, which corresponds to approximately 7 grid points within the current layer half width Δr_{kink}. For the $r_s/R_0 = 0.1$ simulation in Figure 2, the current layer at the mode rational surface Δr_{kink} is very thin. A radially nonuniform grid have also been successfully used so there can be higher resolution near the $q = 1$ surface, and lower resolution away from it.

The internal kink mode growth rate is well converged for 32 grid points in the ζ direction and 300 grid points in the

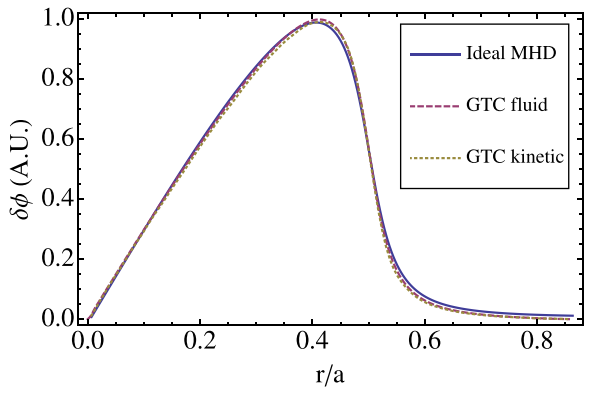

FIG. 4. The mode structure of the electrostatic potential $\delta\phi$ vs. the radial coordinate r/a is plotted for the $r_s/R_0 = 0.25$ case in cylindrical geometry.

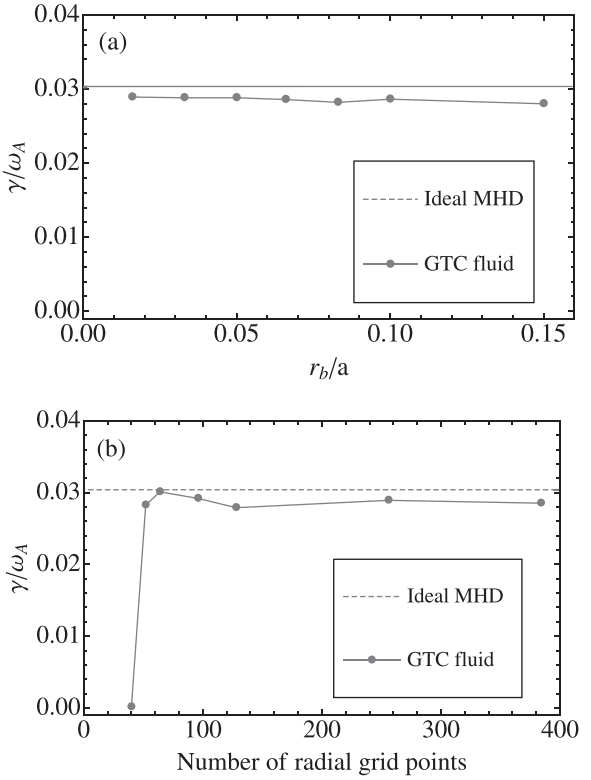

FIG. 5. (a) The growth rate of the internal kink mode is plotted vs. radial position of the FD boundary. (b) The GTC internal kink mode growth rate is plotted against the number of radial grid points.

θ-direction at the $q = 1$ surface. In GTC gyrokinetic simulations of high-n microturbulence, the number of poloidal grid points is determined such that the arc length between grid points is approximately constant on all flux surfaces. This means there are less poloidal grid points near the axis, which is why 300 poloidal grid points at the $q = 1$ surface were needed. For simulations of the low-n modes, it is computationally more efficient to use a uniform grid in the θ-direction, which will be used in the future. For gyrokinetic simulations, ten particles per cell are adequate for convergence.

IV. GTC SIMULATIONS OF KINK INSTABILITY IN TOROIDAL GEOMETRY

Using the analytic toroidal equilibria shown in Eqs. (17) and (18), GTC simulations are performed with the same parameters as the cylindrical simulation to study the effects of toroidicity on internal kink modes with $r_s/R_0 = 0.25$.

A. GTC simulations in fluid limit

When the lowest-order tokamak model shown in Eq. (17) is used, the properties of the internal kink mode are very similar to the cylindrical geometry. The growth rate is $\gamma = 0.026\ \omega_A$, which is approximately the same as the cylindrical geometry growth rate of $\gamma = 0.028\ \omega_A$. Figure 6 shows the electrostatic potential of internal kink mode for the two toroidal geometry models. The kink mode structure for the lowest-order toroidal model (Eq. (17)) is approximately the same as the cylindrical geometry model, and little coupling to higher m harmonics is observed.

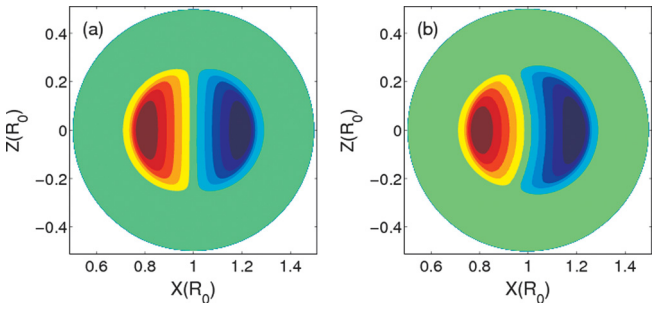

FIG. 6. The poloidal cross section of $\delta\phi$ mode structure is plotted for the lowest-order tokamak equilibrium in (a), and for the realistic tokamak equilibrium in (b).

When the realistic toroidal model shown in Eq. (18) is used, the growth rate is $\gamma = 0.0255\ \omega_A$, which is approximately the same as the lowest order tokamak model of Eq. (18). Figure 6(b) shows that for the realistic toroidal model, the internal kink mode is bent so that the mode is larger on the low field side. This bending is along the magnetic flux coordinate θ such that the internal kink mode is still almost purely an $m = 1$ mode in the flux coordinate system, with little m-mode coupling. Since the only physical difference between the lowest-order tokamak model and the realistic tokamak model is magnetic field configuration, the change to the mode structure must be solely due to the more realistic magnetic field configuration. The growth rates for both toroidal models are approximately the same as the cylindrical geometry model, and only small stabilization due to m-mode coupling as predicted by Bussac *et al.*[18] However, Galvao *et al.* predicted that the kink mode becomes more unstable for a lower aspect ratio case.[19]

B. GTC gyrokinetic simulations

Using the linearized gyrokinetic Eqs. (2)–(12), the realistic toroidal geometry model shown in Eq. (18) is simulated in this section. The ion banana orbit width for this simulation is approximately $\Delta r_{banana} = 2q(R_0/r)^{1/2}\rho_i = 4\rho_i$. Then, the ratio of the ion banana orbit width to the kink current layer width is $\Delta r_{banana}/\Delta r_{kink} \approx 0.12$, so kinetic effects should still be minimal when $\beta_i = 0.4\%$. However, when ion kinetic effects are added to the toroidal geometry simulation, the internal kink mode growth rate decreases significantly to $\gamma = 0.0085\ \omega_A$ compared to the GTC fluid simulation of $\gamma = 0.0255\ \omega_A$ in the same geometry as discussed in Subsection IV A.

To understand the gyrokinetic result, several simulation scans were performed, which are shown in Figure 7. In the first scan, the ion pressure is varied while $\beta_i = \beta_e$ and the parallel electric field $\delta E_{||}$ is kept. The growth rate of the internal kink mode increases as the β_i is reduced, where at very low plasma pressure does the gyrokinetic growth rate reaches the fluid growth rate. In the second scan, the β_i is varied while $\beta_i = \beta_e$ and setting $\delta E_{||} = 0$. The variations of the growth rate are approximately the same as the scan with $\delta E_{||} = 0$. As a third scan, the ion temperature is varied while the electron temperature remains constant with $\beta_e = 0.4\%$, and $\delta E_{||} = 0$. The mode growth rates change is about the same as the previous two scans.

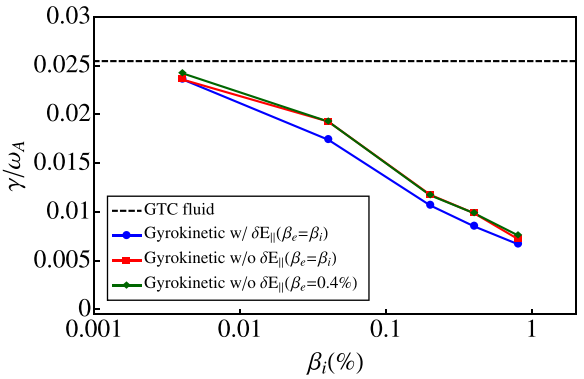

FIG. 7. The growth rate vs. the ion beta β_i.

As a further check to see if this reduction of the growth rate is physical, Figure 8 shows a test excluding ion kinetic effects near the magnetic axis, while retaining kinetic effects in the rest of the simulation domain. In this test, if a particle crosses the boundary between the kinetic region and the region where thermal ion motion is suppressed, it will be reflected back into the kinetic region. When kinetic effects are removed near the $q = 1$ surface, the internal kink mode growth rate jumps from the gyrokinetic growth rate to the fluid growth rate. The kinetic effect that reduces the growth rate is located near the resonant surface, which verifies that this effect is physical.

The fact that the growth rate of the internal kink mode with the parallel electric field turned on and off are about the same suggests the parallel electric field plays little role. The reduction of the growth rate in kinetic simulations is due to ion kinetic effects, even though the banana orbit is much smaller than the MHD current layer. The ion kinetic effects that could cause this stabilization include trapped ions, wave-particle interactions, and polarization drift. Note that while the gyrokinetic eigenvalue calculation by Qin *et al.*[30] was in a regime where the ratio of the banana orbit width to fluid current layer $\Delta r_{banana}/\Delta r_{kink}$ is much larger than our simulation, they also observed that the ion trapped particle orbit can significantly affects the internal kink growth rate.

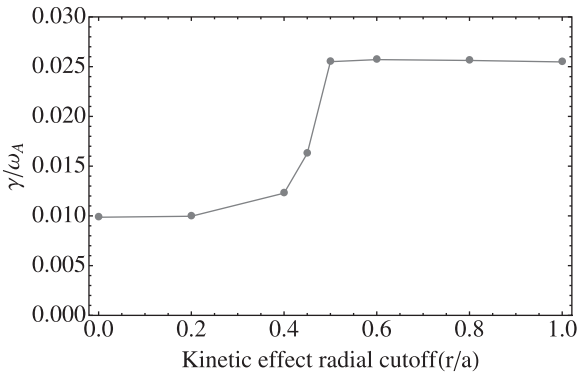

FIG. 8. Internal kink mode growth rate is plotted against the kinetic effects radial cutoff, where kinetic effects are kept only outside the radial cutoff position. Inside the radial cutoff domain, the ion thermal motion is suppressed. Outside of the radial cutoff domain, all kinetic effects are kept.

While this paper has focused on uniform pressure profiles, in simulations with a finite pressure gradient, the pressure gradient can destabilize the internal kink mode.

V. CONCLUSION

In this paper, a method extending the simulation domain to the magnetic axis was implemented in GTC. With this capability, the internal kink mode was simulated in both cylindrical and toroidal geometry. In the cylindrical geometry, the simulations were benchmarked and showed good agreement with ideal MHD. In the toroidal geometry, fluid simulations have a similar growth rate compared to the fluid simulations in the cylindrical geometry. However, for the realistic toroidal geometry model there is a change in mode structure due to the change in magnetic field configuration. When ion kinetic effects are added to the toroidal geometry simulation, the internal kink mode growth rate is significantly reduced even when the radial width of the perturbed current layer is an order of magnitude larger than the banana orbit width. This reduction of growth rate is attributed fully to the ion kinetic effects.

The follow-up paper[39] will discuss the verification of a resistive tearing model in GTC. It will then examine how ion kinetic effects interact with the resistive tearing mode. The future work will extend simulations to the nonlinear regime in order to examine nonlinear effects such as the kink saturation mechanism and generation of zonal fields. The gyrokinetic capabilities developed in these works will also be applied to study more dangerous modes such as fishbone modes and neoclassical tearing modes.

ACKNOWLEDGMENTS

This work was supported by U.S. DOE SciDAC GSEP Center and DOE Grant Nos. DE-FG02-07ER54916 and DE-SC0010416, and used resources of the Oak Ridge Leadership Computing Facility at Oak Ridge National Laboratory (DOE Contract No. DE-AC05-00OR22725), and the National Energy Research Scientific Computing Center (DOE Contract No. DE-AC02-05CH11231).

[1]M. N. Rosenbluth, R. Y. Dagazian, and P. H. Rutherford, "Nonlinear properties of the internal m = 1 kink instability in the cylindrical tokamak," Phys. Fluids **16**(11), 1894–1902 (1973).
[2]H. P. Furth, J. Killeen, and M. N. Rosenbluth, "Finite-resistivity instabilities of a sheet pinch," Phys. Fluids **6**(4), 459 (1963).
[3]K. McGuire, R. Goldston, M. Bell, M. Bitter, K. Bol, K. Brau, D. Buchenauer, T. Crowley, S. Davis, F. Dylla, H. Eubank, H. Fishman, R. Fonck, B. Grek, R. Grimm, R. Hawryluk, H. Hsuan, R. Hulse, R. Izzo, R. Kaita, S. Kaye, H. Kugel, D. Johnson, J. Manickam, D. Manos, D. Mansfield, E. Mazzucato, R. McCann, D. McCune, D. Monticello, R. Motley, D. Mueller, K. Oasa, M. Okabayashi, K. Owens, W. Park, M. Reusch, N. Sauthoff, G. Schmidt, S. Sesnic, J. Strachan, C. Surko, R. Slusher, H. Takahashi, F. Tenney, P. Thomas, H. Towner, J. Valley, and R. White, "Study of high-beta magnetohydrodynamic modes and fast-ion losses in PDX," Phys. Rev. Lett. **50**, 891–895 (1983).
[4]S. von Goeler, W. Stodiek, and N. Sauthoff, "Studies of internal disruptions and $m = 1$ oscillations in tokamak discharges with soft x-ray techniques," Phys. Rev. Lett. **33**, 1201–1203 (1974).
[5]Z. Chang, J. D. Callen, E. D. Fredrickson, R. V. Budny, C. C. Hegna, K. M. McGuire, M. C. Zarnstorff, and TFTR Group, "Observation of nonlinear neoclassical pressure-gradient driven tearing modes in TFTR," Phys. Rev. Lett. **74**, 4663–4666 (1995).
[6]D. Pfirsch and H. Tasso, "A theorem on MHD-instability of plasmas with resistive walls," Nucl. Fusion **11**(3), 259 (1971).
[7]T. C. Hender, J. C. Wesley, J. Bialek, A. Bondeson, A. H. Boozer, R. J. Buttery, A. Garofalo, T. P. Goodman, R. S. Granetz, Y. Gribov, O. Gruber, M. Gryaznevich, G. Giruzzi, S. Günter, N. Hayashi, P. Helander, C. C. Hegna, D. F. Howell, D. A. Humphreys, G. T. A. Huysmans, A. W. Hyatt, A. Isayama, S. C. Jardin, Y. Kawano, A. Kellman, C. Kessel, H. R. Koslowski, R. J. La Haye, E. Lazzaro, Y. Q. Liu, V. Lukash, J. Manickam, S. Medvedev, V. Mertens, S. V. Mirnov, Y. Nakamura, G. Navratil, M. Okabayashi, T. Ozeki, R. Paccagnella, G. Pautasso, F. Porcelli, V. D. Pustovitov, V. Riccardo, M. Sato, O. Sauter, M. J. Schaffer, M. Shimada, P. Sonato, E. J. Strait, M. Sugihara, M. Takechi, A. D. Turnbull, E. Westerhof, D. G. Whyte, R. Yoshino, H. Zohm, Disruption the ITPA MHD, and Magnetic Control Topical Group, "MHD stability, operational limits and disruptions," Nucl. Fusion **47**(6), S128 (2007).
[8]X.-Q. Wang, R.-B. Zhang, L. Qin, and X.-G. Wang, "Non-resonant fishbone instabilities of q min1 in tokamak plasmas with weakly reversed magnetic shear," Plasma Phys. Controlled Fusion **56**(9), 095013 (2014).
[9]H. Cai and G. Fu, "Hybrid simulation of energetic particle effects on tearing modes in tokamak plasmas," Phys. Plasmas **19**(7), 072506 (2012).
[10]C. C. Kim and the NIMROD Team, "Impact of velocity space distribution on hybrid kinetic-magnetohydrodynamic simulation of the (1,1) mode," Phys. Plasmas **15**(7), 072507 (2008).
[11]Q. Yu and S. Gunter, "Locking of neoclassical tearing modes by error fields and its stabilization by rf current," Nucl. Fusion **48**(6), 065004 (2008).
[12]W. W. Lee, "Gyrokinetic approach in particle simulation," Phys. Fluids **26**(2), 556 (1983).
[13]K. L. Wong, M. S. Chu, T. C. Luce, C. C. Petty, P. A. Politzer, R. Prater, L. Chen, R. W. Harvey, M. E. Austin, L. C. Johnson, R. J. La Haye, and R. T. Snider, "Internal kink instability during off-axis electron cyclotron current drive in the DIII-D tokamak," Phys. Rev. Lett. **85**, 996–999 (2000).
[14]W. W. Heidbrink, M. E. Austin, R. K. Fisher, M. García-Muñoz, G. Matsunaga, G. R. McKee, R. A. Moyer, C. M. Muscatello, M. Okabayashi, D. C. Pace, K. Shinohara, W. M. Solomon, E. J. Strait, M. A. Van Zeeland, and Y. B. Zhu, "Characterization of off-axis fishbones," Plasma Phys. Controlled Fusion **53**(8), 085028 (2011).
[15]I. T. Chapman, R. J. La Haye, R. J. Buttery, W. W. Heidbrink, G. L. Jackson, C. M. Muscatello, C. C. Petty, R. I. Pinsker, B. J. Tobias, and F. Turco, "Sawtooth control using electron cyclotron current drive in iter demonstration plasmas in DIII-D," Nucl. Fusion **52**(6), 063006 (2012).
[16]J. E. Menard, R. E. Bell, D. A. Gates, S. M. Kaye, B. P. LeBlanc, F. M. Levinton, S. S. Medley, S. A. Sabbagh, D. Stutman, K. Tritz, and H. Yuh, "Observation of instability-induced current redistribution in a spherical-torus plasma," Phys. Rev. Lett. **97**, 095002 (2006).
[17]I. T. Chapman, M.-D. Hua, S. D. Pinches, R. J. Akers, A. R. Field, J. P. Graves, R. J. Hastie, C. A. Michael, and the MAST Team, "Saturated ideal modes in advanced tokamak regimes in mast," Nucl. Fusion **50**(4), 045007 (2010).
[18]M. N. Bussac, R. Pellat, D. Edery, and J. L. Soule, "Internal kink modes in toroidal plasmas with circular cross sections," Phys. Rev. Lett. **35**(24), 1638–1641 (1975).
[19]R. M. O. Galvão, P. H. Sakanaka, and H. Shigueoka, "Influence of toroidal effects on the stability of the internal kink mode," Phys. Rev. Lett. **41**, 870–873 (1978).
[20]W. Kerner, R. Gruber, and F. Troyon, "Numerical study of the internal kink mode in tokamaks," Phys. Rev. Lett. **44**, 536–540 (1980).
[21]J. Manickam, "Stability of n = 1 internal modes in tokamaks," Nucl. Fusion **24**(5), 595 (1984).
[22]F. D. Halpern, D. Leblond, H. Lütjens, and J.-F. Luciani, "Oscillation regimes of the internal kink mode in tokamak plasmas," Plasma Phys. Controlled Fusion **53**(1), 015011 (2011).
[23]G. Ara, B. Basu, B. Coppi, G. Laval, M. N. Rosenbluth, and B. V. Waddell, "Magnetic reconnection and m = 1 oscillations in current carrying plasmas," Ann. Phys. **112**(2), 443–476 (1978).
[24]J. F. Drake, "Kinetic theory of m = 1 internal instabilities," Phys. Fluids **21**(10), 1777–1789 (1978).
[25]G. Y. Fu, W. Park, H. R. Strauss, J. Breslau, J. Chen, S. Jardin, and L. E. Sugiyama, "Global hybrid simulations of energetic particle effects on the n = 1 mode in tokamaks: Internal kink and fishbone instability," Phys. Plasmas **13**(5), 052517 (2006).

[26]L. Chen, R. B. White, and M. N. Rosenbluth, "Excitation of internal kink modes by trapped energetic beam ions," Phys. Rev. Lett. **52**, 1122–1125 (1984).
[27]H. Naitou, K. Tsuda, W. W. Lee, and R. D. Sydora, "Gyrokinetic simulation of internal kink modes," Phys. Plasmas **2**(11), 4257–4268 (1995).
[28]H. Naitou, Y. Yamada, K. Kajiwara, W. li Lee, S. Tokuda, and M. Yagi, "Global and kinetic mhd simulation by the Gpic-MHD code," Plasma Sci. Technol. **13**(5), 528 (2011).
[29]A. Mishchenko and A. Zocco, "Global gyrokinetic particle-in-cell simulations of internal kink instabilities," Phys. Plasmas **19**(12), 122104 (2012).
[30]H. Qin, W. M. Tang, and G. Rewoldt, "Linear gyrokinetic theory for kinetic magnetohydrodynamic eigenmodes in tokamak plasmas," Phys. Plasmas **6**(6), 2544–2562 (1999).
[31]Z. Lin, T. S. Hahm, W. W. Lee, W. M. Tang, and R. B. White, "Turbulent transport reduction by zonal flows: Massively parallel simulations," Science **281**(5384), 1835–1837 (1998).
[32]I. Holod, W. L. Zhang, Y. Xiao, and Z. Lin, "Electromagnetic formulation of global gyrokinetic particle simulation in toroidal geometry," Phys. Plasmas **16**(12), 122307 (2009).
[33]Z. Lin, I. Holod, L. Chen, P. H. Diamond, T. S. Hahm, and S. Ethier, "Wave-particle decorrelation and transport of anisotropic turbulence in collisionless plasmas," Phys. Rev. Lett. **99**, 265003 (2007).
[34]Y. Xiao and Z. Lin, "Turbulent transport of trapped-electron modes in collisionless plasmas," Phys. Rev. Lett. **103**, 085004 (2009).
[35]W. Zhang, Z. Lin, and L. Chen, "Transport of energetic particles by microturbulence in magnetized plasmas," Phys. Rev. Lett. **101**, 095001 (2008).
[36]H. S. Zhang, Z. Lin, and I. Holod, "Nonlinear frequency oscillation of alfvén eigenmodes in fusion plasmas," Phys. Rev. Lett. **109**, 025001 (2012).
[37]Z. Wang, Z. Lin, I. Holod, W. W. Heidbrink, B. Tobias, M. Van Zeeland, and M. E. Austin, "Radial localization of toroidicity-induced alfvén eigenmodes," Phys. Rev. Lett. **111**, 145003 (2013).
[38]W. Deng, Z. Lin, and I. Holod, "Gyrokinetic simulation model for kinetic magnetohydrodynamic processes in magnetized plasmas," Nucl. Fusion **52**(2), 023005 (2012).
[39]D. Liu *et al.*, Phys. Plasmas **21**, 122520 (2014).
[40]W. W. Lee, "Gyrokinetic particle simulation model," J. Comput. Phys. **72**(1), 243–269 (1987).
[41]A. J. Brizard and T. S. Hahm, "Foundations of nonlinear gyrokinetic theory," Rev. Mod. Phys. **79**, 421–468 (2007).
[42]A. M. Dimits, "Gyrokinetic equations in an extended orderinga," Phys. Plasmas **17**(5), 055901 (2010).
[43]Z. Lin and L. Chen, "A fluid-kinetic hybrid electron model for electromagnetic simulations," Phys. Plasmas **8**(5), 1447 (2001).
[44]J. C. Cummings, Ph.D. dissertation, Princeton University, 1995.
[45]D. Liu and L. Chen, "A finite-mass fluid electron simulation model for low-frequency electromagnetic waves in magnetized plasmas," Plasma Phys. Controlled Fusion **53**(6), 062002 (2011).
[46]R. B. White, A. H. Boozer, and R. Hay, "Drift Hamiltonian in magnetic coordinates," Phys. Fluids **25**(3), 575–576 (1982).
[47]Y. Xiao *et al.*, "Gyrokinetic particle simulation of microturbulence for general geometry and experimental profiles" (submitted).
[48]L. Zhihong, S. Ethier, T. S. Hahm, and W. M. Tang, "Verification of gyrokinetic particle simulation of device size scaling of turbulent transport," Plasma Sci. Technol. **14**(12), 1125 (2012).
[49]J. P. Goedbloed and H. J. L. Hagebeuk, "Growth rates of instabilities of a diffuse linear pinch," Phys. Fluids **15**(6), 1090–1101 (1972).